# Confinement-induced orientational alignment of quasi-2D fluids

A Letters Journal Exploring the Frontiers of Physics

June 2009

EPL, **86** (2009) 66001
doi: 10.1209/0295-5075/86/66001

www.epljournal.org

# Confinement-induced orientational alignment of quasi-2D fluids

K. Nygård[1(a)], D. K. Satapathy[1], J. Buitenhuis[2], E. Perret[1], O. Bunk[1], C. David[1] and J. F. van der Veen[1,3]

[1] *Research Department of Synchrotron Radiation and Nanotechnology, Paul Scherrer Institut CH-5232 Villigen PSI, Switzerland*
[2] *Institute of Solid State Research, Forschungszentrum Jülich - D-52425 Jülich, Germany, EU*
[3] *ETH Zürich - CH-8093 Zürich, Switzerland*

received 8 May 2009; accepted in final form 3 June 2009
published online 17 June 2009

PACS 68.08.-p – Liquid-solid interfaces
PACS 61.05.cf – X-ray scattering (including small-angle scattering)
PACS 82.70.-y – Disperse systems; complex fluids

**Abstract** – We have developed a unique approach for studying the ensemble-averaged nearest-neighbor coordination of confined fluids by combining small-angle X-ray scattering and phase-retrieval–based X-ray diffraction from fluid-filled nanofluidic channel arrays. We apply the method to a charge-stabilized quasi–two-dimensional colloidal fluid (particle diameter 48 nm), focusing on the structural transition from a monolayer to a bilayer with increasing fluid film thickness. In contrast to theoretical work on the paradigmatic hard-sphere fluid, we find unambiguous experimental evidence for orientational alignment of fluids in extreme confinement.



Nano-scale fluids in extreme confinement are ubiquitous in nature and in technological applications, the examples ranging from proteins in narrow pores to micro- and nanofluidic devices. Restricting one of the spatial dimensions to only a few times the particle diameter induces ordering, and thus affects macroscopic properties such as the diffusion of the fluid constituents [1]. Consequently, confined fluids have gathered considerable theoretical interest [2–4]. However, experimental studies on nano-scale fluids are hampered by the wavelength limitations of the traditionally used optical microscopy [5]. Hard X-rays can overcome this obstacle, as demonstrated by proof-of-principle experiments using waveguiding [6] and reflectivity [7] techniques. More recently, phase-retrieval–based X-ray diffraction (XRD) from fluid-filled channel arrays has been shown to yield the out-of-plane (*i.e.*, perpendicular to the confining surfaces), ensemble-averaged fluid density profile in a model-independent manner [8,9]. The local structure (*i.e.*, the two-point density correlation function), in turn, can be studied by small-angle X-ray scattering (SAXS), providing ensemble-averaged information on the nearest-neighbor coordination in terms of the structure factor $S(\mathbf{q})$, *i.e.*, the reciprocal-space counterpart of the pair distribution function $g(\mathbf{r})$. The technique has previously been used, *e.g.*, to observe five-fold local symmetry in liquid lead at the solid-liquid interface [10]. However, experimental work on confined fluids has hitherto been hampered by a complicated characterization of the confining mesostructured porous silicates [11].

In this letter, we report synchrotron-radiation–based SAXS studies on the local structure of a charge-stabilized colloidal fluid with one of the spatial dimensions being restricted to a few times the particle diameter. For confinement we use well-characterized nanofluidic channel arrays (*i.e.*, in effect diffraction gratings). This approach makes reliable modeling of the excluded-volume effects due to the parallel, confining surfaces feasible, facilitating the interpretation of the observed changes in the structure factor. Moreover, the use of such channel arrays serves two additional purposes: first, the scattering volume is 1000-fold compared to using a single channel for confinement (in the present study approximately 20 picolitres), making the present SAXS studies on confined fluids feasible. Second, the channel arrays allow simultaneous reconstruction of the out-of-plane fluid density profile by XRD using phase-retrieval methods [8,9]. Such experimental information is essential for an accurate theoretical description of the two-point density correlation function [3] (and hence $g(\mathbf{r})$ or $S(\mathbf{q})$). The main finding of this study can be summarized as follows: contrariwise to theoretical work on hard-sphere fluids [4], the present quasi–two-dimensional (quasi-2D) fluid is found to exhibit confinement-induced orientational alignment.

(a) E-mail: kim.nygard@psi.ch

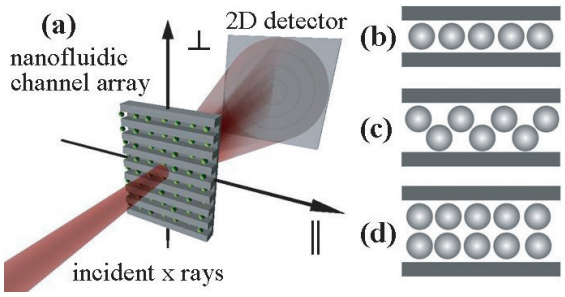


Fig. 1: (Colour on-line) Schematic of (a) experimental setup, (b) a monolayer, (c) a buckled monolayer, and (d) a bilayer.

Colloids, with tunable properties such as particle sizes and interactions, are frequently used as model systems in condensed-matter physics. Here we studied an opaque suspension consisting of negatively charged spherical $SiO_2$ nanoparticles dispersed in a solution of dimethylformamide and 0.5 mM of LiCl (see below for details on the *in situ* SAXS characterization of the bulk fluid). Details on the synthesis of the colloids can be found elsewhere [12,13].

For confinement we used a silicon-based nanofluidic chip, the fabrication of which has been described elsewhere [9,14]. It consisted of several high-aspect-ratio channel arrays with a period of 400 nm, a height of 2.4 $\mu$m, and a systematically varied channel width in the range 127–186 nm. Each array was composed of more than 1000 identical, rectangular channels, with a total area of $0.5 \times 0.5\,\mathrm{mm}^2$. Holes with the size of the arrays were also included, allowing *in situ* SAXS characterization of the bulk fluid. The nanofluidic chip was mounted on a glass slide, in order to prevent evaporation of the fluid. The resulting fluid reservoir between the glass slide and the channel array allowed a free exchange of particles and ions. Since the channel arrays were covered by a natural oxide layer, they had a negative surface charge, similar to the colloidal particles.

The experiment was conducted at the cSAXS beam line (X12SA) of the Swiss Light Source (see fig. 1(a) for a schematic of the experimental setup). The incident X-rays impinged perpendicular to the channel array, and the scattered X-rays were collected in transmission geometry 7 m behind the sample using a single-photon-counting, 2D pixel detector (Pilatus 2M, $1461 \times 1560$ pixels with a size of $172 \times 172\,\mu\mathrm{m}^2$ each). The incident X-ray wavelength was $\lambda = 0.100$ nm and the beam size at the sample was approximately $0.2(\mathrm{H}) \times 0.1(\mathrm{V})\,\mathrm{mm}^2$. An evacuated flight tube was positioned between the sample and the detector in order to minimize parasitic scattering. Accurate scattering data were collected both from the empty channel arrays and the fluid reservoir, thus allowing a reliable background subtraction. Moreover, XRD data from the fluid-filled channel arrays were collected up to typically 50 diffraction orders (see ref. [9] for a representative diffraction pattern), allowing a reconstruction of the out-of-plane fluid density profile with a real-space sampling of approximately 4 nm.

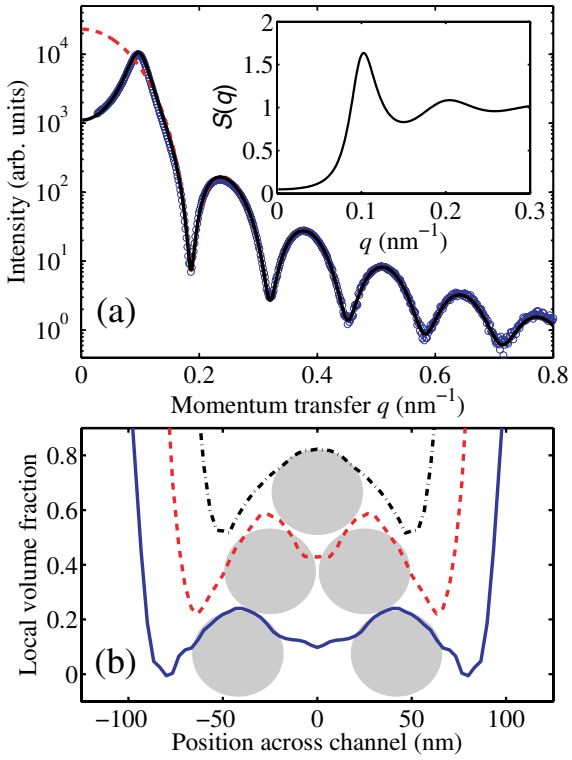


Fig. 2: (Colour on-line) Fluid characterization: (a) SAXS data from the bulk fluid. The solid (dashed) line depicts a model of polydisperse particles with (without) interactions. Inset: isotropic structure factor $S(q)$. (b) Out-of-plane local volume fraction of particles for confining channel widths of 186 (solid line), 153 (dashed line), and 127 nm (dash-dotted line, each vertically offset by 0.25). The nearly vertical lines denote the confining surfaces, with the tapering being an artefact due to dynamic diffraction effects [15], while the spheres indicate the particle size (radius $R = 24.1$ nm).

The SAXS data acquired from the bulk fluid are presented in fig. 2(a). The modeling is carried out within the decoupling approximation [16] using the form factor of spherical particles, with the polydispersity of the particles being accounted for using the Schultz-Flory distribution [17]. The fit (in the range $0.3\,\mathrm{nm}^{-1} \leqslant q \leqslant 1.0\,\mathrm{nm}^{-1}$) yields the average particle radius $R = 24.1 \pm 0.1$ nm and the polydispersity $\Delta R/R = 0.038 \pm 0.002$ (*i.e.*, in effect a Gaussian distribution with a variance $\sigma^2 = 0.42 \pm 0.04\,\mathrm{nm}^2$), in reasonable agreement with transmission electron microscopy results. Next, the particle-particle interactions are modeled using screened Coulomb repulsions within the rescaled mean spherical approximation [18,19]. The fit (in the range $q \geqslant 0.03\,\mathrm{nm}^{-1}$) gives the Debye screening length $\kappa^{-1} = 8.4$ nm and the particle volume fraction $\Phi = 0.167$. The latter value is in excellent agreement with $\Phi = 0.172 \pm 0.004$ independently obtained from the efficiencies of the diffraction orders. In order to facilitate the analysis of the confined fluid

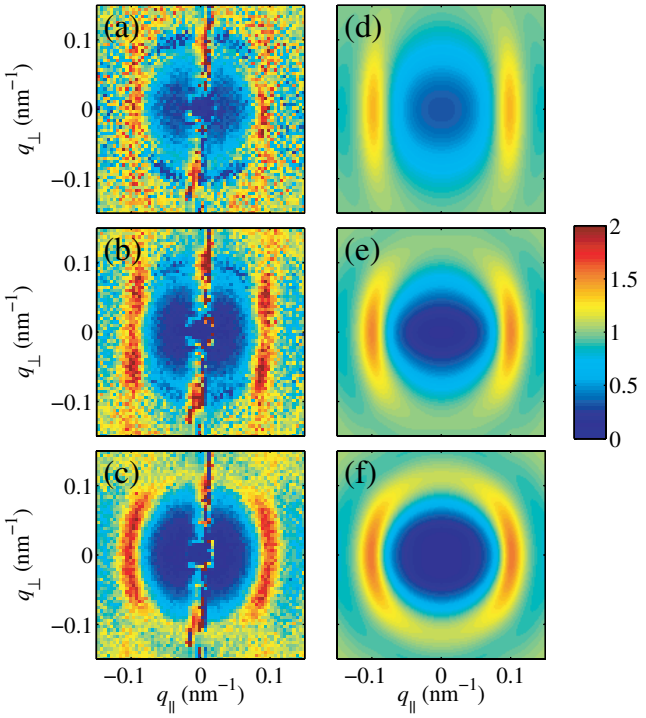


Fig. 3: (Colour on-line) Confinement-induced anisotropic structure factor $S(q_\perp, q_\parallel)$: experimental data (rotated clockwise by 3°) for (a) 127, (b) 153, and (c) 186 nm channel widths, and model calculations (see text for details) for (d) 87, (e) 113, and (f) 146 nm channel widths.

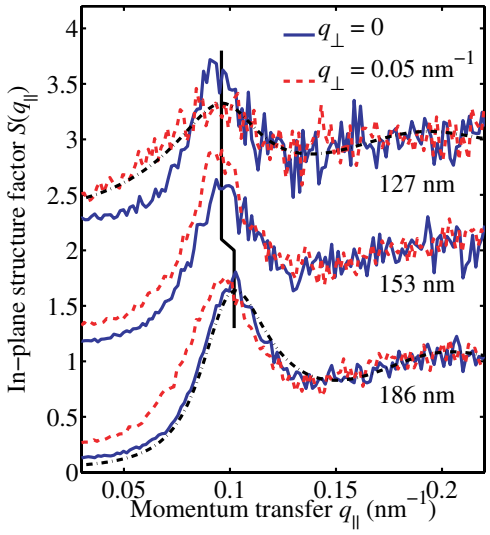


Fig. 4: (Colour on-line) In-plane structure factor $S(q_\parallel)$ for channel widths of 127, 153, and 186 nm (each vertically offset by 1.0) for selected out-of-plane momentum transfers. The dash-dotted lines denote the 2D (vertically offset) and 3D $S(q)$ for comparison. The vertical line depicts the position of the first maximum in $S(q_\parallel)$ for $q_\perp = 0$.

data (see below), we define the effective particle radius $R_{\text{eff}} = 34.0$ nm, as determined from the first peak position in the isotropic $g(r)$ obtained from the fit.

To characterize the confined fluid, we have also determined the out-of-plane fluid density profile by XRD from the fluid-filled channel array using an iterative phase-retrieval algorithm [8,20]. The density profile is presented in fig. 2(b) as the local particle volume fraction (convoluted with the projection of the particles spherical shape) for channel widths of 127, 153, and 186 nm. The data reflect the transition from a monolayer (fig. 1(b)) to a bilayer (fig. 1(d)) with increasing channel width. Two effects in particular should be noted: First, a depletion of particles is observed close to the solid-fluid interface. This effect can be attributed to the net result of the electrostatic repulsions between the charged particles as well as the particles and the like-charged confining surfaces [21]. Second, although a doubly peaked density profile is observed for the channel width of 153 nm, the out-of-plane distance between the two layers (denoted $r_\perp$) is smaller than the effective particle diameter, implying a buckled monolayer (fig. 1(c)).

Next we turn to the SAXS data collected from the confined fluid. Figure 3 presents the confinement-induced anisotropic structure factor $S(q_\perp, q_\parallel)$ (obtained by dividing out the square modulus of the form factor determined from fig. 2(a)) as a function of in-plane $q_\parallel$ (*i.e.*, parallel to the confining surfaces) and out-of-plane $q_\perp$ momentum transfers for channel widths of 127, 153, and 186 nm (see footnote[1]). The data around $q_\parallel = 0$ are influenced by the beam stop and diffraction from the channel array, and should therefore be neglected in the following discussion. Notably, $S(q_\perp, q_\parallel)$ is found to be distinctly different upon increasing the confining channel width to 186 nm: the transition from a (buckled) monolayer to a bilayer is manifest in the elongation of the first maximum in $S(q_\perp, q_\parallel)$ along the out-of-plane direction. We have confirmed this observation for several channel widths both below and above the transition.

In order to facilitate the analysis of our experimental data, we also present in fig. 4 the corresponding in-plane structure factors $S(q_\parallel)$ (*i.e.*, constant-$q_\perp$ sections of $S(q_\perp, q_\parallel)$) for out-of-plane momentum transfers $q_\perp = 0$ and $q_\perp = 0.05\,\text{nm}^{-1}$. We note that the value of the first maximum in $S(q_\parallel)$, denoted $S(q_{\text{max}}^{\text{1st}})$, is well below the Hansen-Verlet criterion for freezing [22] (which is $S(q_{\text{max}}^{\text{1st}}) \approx 5$ and $S(q_{\text{max}}^{\text{1st}}) \approx 2.85$ for the limiting 2D and three-dimensional (3D) cases, respectively), indicating that the confined colloid is in the liquid state. Moreover, the transition from a (buckled) monolayer to a bilayer is observed in the shift $q_{\text{max}}^{\text{1st}} \approx 0.097\,\text{nm}^{-1} \to 0.103\,\text{nm}^{-1}$ of the first maximum in $S(q_\parallel)$ (see vertical line). This observation (and the elongation of the first maximum in $S(q_\perp, q_\parallel)$ along the out-of-plane direction as observed in fig. 3) is a trivial effect of dimensionality and can be rationalized in terms of different Jacobians in the Fourier

[1]We note that dynamical effects in the SAXS data due to a non-planar wave field inside the channel [15] are minor.

transform of $g(\mathbf{r})$, as has previously been done for SAXS data acquired from a monolayer of liquid lead [23]: in the limiting 2D and 3D cases, the Fourier transforms of the isotropic $g(r)$ are the so-called Fourier-Bessel and Fourier-sine transforms, respectively. For comparison, these 2D and 3D $S(q)$ are shown in fig. 4 using the isotropic $g(r)$ determined from fig. 2(a). The remarkable agreement in terms of the peak position of the first maximum between the 2D and 3D $S(q)$ and the experimental $S(q_\parallel)$ (for $q_\perp = 0$) suggests a negligible effect of confinement on $R_{\text{eff}}$.

In order to corroborate the above interpretation, we have also analyzed the experimental data in terms of model calculations. The structure factor of the confined fluid can formally be written as [24]

$$S(\mathbf{q}) \simeq 1 + \frac{1}{N} \iint n(x_1) n(x_1 + x) \left[ g(\mathbf{r}) - 1 \right] \mathrm{e}^{i\mathbf{q}\cdot\mathbf{r}} \mathrm{d}^3\mathbf{r}_1 \mathrm{d}^3\mathbf{r}, \tag{1}$$

with $N$ denoting the number of particles and $n(x)$ the in-plane–averaged number density. The particle position in the channel and the corresponding out-of-plane component are depicted by $\mathbf{r}_1$ and $x_1$, respectively, while $\mathbf{r}$ and $x$ denote translations with respect to $\mathbf{r}_1$ and $x_1$. The model $S(q_\perp, q_\parallel)$ is readily obtained in the limit of a constant $n(x)$ within the channel [24], *i.e.*, including only the excluded volume due to structureless, hard surfaces and utilizing the isotropic $g(r)$ determined from fig. 2(a). This model essentially accounts for the channel-width–dependent Jacobian in the Fourier transform of $g(r)$. Since the model neglects electrostatic interactions between the particles and the confining surfaces, the depletion of particles at the solid-fluid interface is effectively included using a narrower channel width. The model is presented in fig. 3(f) for a channel width of 146 nm, *i.e.*, assuming a depletion of particles within $2(R_{\text{eff}} - R) \approx 20$ nm from the solid-fluid interface. It qualitatively reproduces the reduced and slightly shifted first peak in the out-of-plane direction of the corresponding experimental data (fig. 3(c)). In order to reproduce the experimental $S(q_\perp, q_\parallel)$ for narrower confinement, however, a channel width less than twice the effective particle diameter must be assumed, as exemplified in figs. 3(d) and (e) for channel widths of 87 and 113 nm (cf. the corresponding experimental data of figs. 3(a) and (b)). The good agreement between experiment and model calculations confirms that the dominant confinement effect in fig. 3 can be attributed to the excluded volume due to the confining surfaces, including the particle depletion at the solid-fluid interface.

The experimental structure factor $S(q_\perp, q_\parallel)$ exhibits a distinct modulation of the first peak with $q_\perp$ for intermediate channel widths $w \approx 142$–$165$ nm (*i.e.*, for $r_\perp / 2R_{\text{eff}} \approx 0.6$–$1.0$). For clarity, this is shown in fig. 5 as a magnified view of the experimental data of fig. 3(b). We note that the first maximum in $S(q_\perp, q_\parallel)$ is found to be $S(q_{\text{max}}^{\text{1st}}) \approx 1.6$ and $S(q_{\text{max}}^{\text{1st}}) \approx 1.9$ for the out-of-plane momentum transfers $q_\perp = 0$ and $q_\perp = 0.06\,\text{nm}^{-1}$ (the latter being the maximum value). In contrast to previous SAXS studies of,

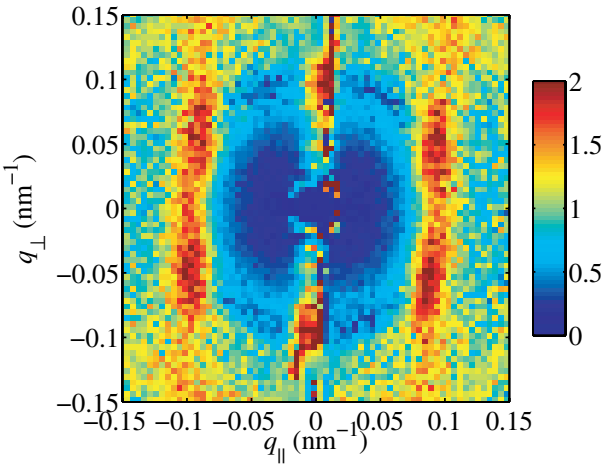


Fig. 5: (Colour on-line) Magnified view of the experimental anisotropic structure factor $S(q_\perp, q_\parallel)$ of fig. 3(b).

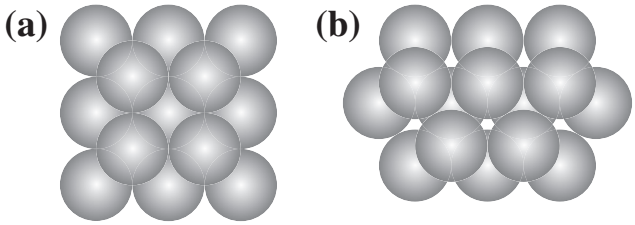


Fig. 6: Schematic top view of two colloidal layers exhibiting (a) square (2□) and (b) hexagonal (2△) symmetry.

*e.g.*, liquid lead on solid substrates [10,23], this modulation is not induced by the (atomic-scale) granularity of the confining surfaces. Although we are not probing the in-plane structure directly, the present interference phenomenon can only be explained in terms of a confinement-induced orientational alignment, with the two colloidal layers exhibiting local spatial correlations. This finding, which is due to a complex interplay between particle-particle (cf. inset of fig. 2(a)) and particle-surface (cf. fig. 2(b)) interactions [2,3], can be understood as follows: dense hard-sphere colloids confined to a film thickness in the range $r_\perp / 2R \approx 0.6$–$1.0$ crystallize into two layers of either square (denoted 2□) or hexagonal (denoted 2△) symmetry, with the particles residing in the hollow sites of the other layer [4] (see fig. 6 for a schematic top view of the 2□ and 2△ symmetries). This phenomenon is expected also for charged particles [25]. In this extreme limit of in-plane long-range positional order, eq. (1) would yield the intensity modulation $I_{hk}(q_\perp)$ along the Bragg rods as observed by grazing-incidence XRD:

$$I_{hk}(q_\perp) \propto \left| \sum \exp\left[ i2\pi(hy_j + kz_j) + iq_\perp \xi_j \right] \right|^2. \tag{2}$$

Here $h$ and $k$ are Miller indices, $y_j$ and $z_j$ fractional in-plane particle positions, $\xi_j$ the out-of-plane particle position, and the sum runs over all particles $j$ in the unit cell. Inserting the particle positions $(y_1, z_1, \xi_1) = (0, 0, 0)$,

$(y_2^{2\square}, z_2^{2\square}, \xi_2^{2\square}) = (1/2, 1/2, r_\perp)$, and $(y_2^{2\triangle}, z_2^{2\triangle}, \xi_2^{2\triangle}) = (1/3, 2/3, r_\perp)$, the intensity modulation of the first Bragg rod $\{10\}$ becomes $I_{\{10\}}^{2\square}(q_\perp) \propto 1 - \cos(q_\perp r_\perp)$ and $I_{\{10\}}^{2\triangle}(q_\perp) \propto 1 - (1/2)\cos(q_\perp r_\perp)$ for the $2\square$ and $2\triangle$ phases, respectively. Both the $2\square$ and $2\triangle$ phases exhibit a maximum in the first Bragg rod at $q_\perp^{\max} = \pi/r_\perp$. Using $r_\perp \approx 53\,\mathrm{nm}$ as determined from fig. 2(b), we obtain $q_\perp^{\max} \approx 0.06\,\mathrm{nm}^{-1}$, in excellent agreement with the experimental data of fig. 5. We further note that the volume fraction of the buckled monolayer is between the volume fractions $\Phi_{2\square} = 0.164$ and $\Phi_{2\triangle} = 0.189$ determined for the $2\square$ and $2\triangle$ phases using the nearest-neighbor distance $2R_{\mathrm{eff}}$. These observations imply a quasi-2D fluid exhibiting both $2\square$- and $2\triangle$-type local structures (*i.e.*, locally square and hexagonal in-plane symmetries as shown in fig. 6, with the particles residing in the hollow sites of the other layer) and a typical out-of-plane orientation angle $\theta = \arctan(r_\perp/R_{\mathrm{eff}}) \approx 57°$. It should be noted that no such orientational alignment has been observed in theoretical studies on confined hard-sphere fluids [4]. In order to verify our experimentally obtained picture of the nearest-neighbor coordination, we foresee quantitative analysis (including electrostatic interactions) using integral [2] and density-functional [3] theories or Monte Carlo simulations [4,25].

Finally, we note that the present method of combining SAXS and phase-retrieval–based XRD from nanofluidic channel arrays is neither wavelength limited nor restricted to optically transparent samples, and is therefore applicable to a variety of nano-scale materials. Future work could focus not only on confined fluids as presented here, but also, *e.g.*, on thin polymer films.

* * *

This work was performed at the Swiss Light Source, Paul Scherrer Institut, Villigen, Switzerland.

REFERENCES


[1] Mittal J., Truskett T. M., Errington J. R. and Hummer G., *Phys. Rev. Lett.*, **100** (2008) 145901.

[2] Kjellander R. and Sarman S., *J. Chem. Soc. Faraday Trans.*, **87** (1991) 1869.

[3] Götzelmann B. and Dietrich S., *Phys. Rev. E*, **55** (1997) 2993.

[4] Schmidt M. and Löwen H., *Phys. Rev. E*, **55** (1997) 7228.

[5] Grier D. G. and Han Y., *J. Phys.: Condens. Matter*, **16** (2004) S4145.

[6] Zwanenburg M. J., Bongaerts J. H. H., Peters J. F., Riese D. O. and van der Veen J. F., *Phys. Rev. Lett.*, **85** (2000) 5154.

[7] Seeck O. H., Kim H., Lee D. R., Shu D., Kaendler I. D., Basu J. K. and Sinha S. K., *Europhys. Lett.*, **60** (2002) 376.

[8] Bunk O., Diaz A., Pfeiffer F., David C., Padeste C., Keymeulen H., Willmott P. R., Patterson B. D., Schmitt B., Satapathy D. K., van der Veen J. F., Guo H. and Wegdam G. H., *Phys. Rev. E*, **75** (2007) 021501.

[9] Nygård K., Satapathy D. K., Bunk O., Diaz A., Perret E., Buitenhuis J., Pfeiffer F., David C. and van der Veen J. F., *Opt. Express*, **16** (2008) 20522.

[10] Reichert H., Klein O., Dosch H., Denk M., Honkimäki V., Lippmann T. and Reiter G., *Nature*, **408** (2000) 839.

[11] Soper A. K., Bruni F. and Ricci M. A., *J. Chem. Phys.*, **109** (1998) 1486.

[12] Osseo-Asare K. and Arriagada F. J., *Colloids Surf.*, **50** (1990) 321.

[13] Arriagada F. J. and Osseo-Asare K., *J. Colloid Interface Sci.*, **211** (1999) 210.

[14] Diaz A., David C., Guo H., Keymeulen H., Pfeiffer F., Wegdam G., Weitkamp T. and van der Veen J. F., *Physica B*, **357** (2005) 199.

[15] Nygård K., Satapathy D. K., Bunk O., Pfeiffer F., David C. and van der Veen J. F., *Appl. Phys. Lett.*, **92** (2008) 214105.

[16] Kotlarchyk M. and Chen S.-H., *J. Chem. Phys.*, **79** (1983) 2461.

[17] Borchert H., Shevchenko E. V., Robert A., Mekis I., Kornowski A., Grübel G. and Weller H., *Langmuir*, **21** (2005) 1931.

[18] Hayter J. B. and Penfold J., *Mol. Phys.*, **42** (1981) 109.

[19] Hansen J.-P. and Hayter J. B., *Mol. Phys.*, **46** (1982) 651.

[20] Bunk O., Diaz A., Pfeiffer F., David C., Schmitt B., Satapathy D. K. and van der Veen J. F., *Acta Crystallogr. A*, **63** (2007) 306.

[21] Satapathy D. K., Bunk O., Jefimovs K., Nygård K., Guo H., Diaz A., Perret E., Pfeiffer F., David C., Wegdam G. H. and van der Veen J. F., *Phys. Rev. Lett.*, **101** (2008) 136103.

[22] Hansen J.-P. and Verlet L., *Phys. Rev.*, **184** (1969) 151.

[23] Grey F., Feidenhans'l R., Pedersen J. S., Nielsen M. and Johnson R. L., *Phys. Rev. B*, **41** (1990) 9519.

[24] Diaz A. and van der Veen J. F., *Thin Solid Films*, **515** (2007) 5645.

[25] Grandner S. and Klapp S. H. L., *J. Chem. Phys.*, **129** (2008) 244703.